sciendo
ISSN 1335-8871
MEASUREMENT SCIENCE REVIEW
Journal homepage: https://content.sciendo.com

The Effect of Differential Pressure and Permanent Pressure Loss on Multi-Hole Orifice Plate

Hariguru TM*, Srinivasan S

Madras Institute of Technology, Department of Instrumentation Engineering, Anna University, Chrompet, 600044, Chennai, India, harigurutm07@gmail.com

Abstract: The widely used orifice plate falls under restricted type flow devices, has the highest differential pressure and permanent pressure drop in the ensemble. The objective is to curtail the permanent pressure drop and maintain the differential pressure across the orifice plate, and thereby, the power required to pump the liquid is retrenched. So, three-hole, four-hole and five-hole orifice plates with an identical area to that of the single-hole orifice plate were designed and experiments were carried out. It is observed that the experimental results almost matched with the simulation data. In comparing the performance, the four-hole orifice plate yielded a higher differential pressure and higher-pressure loss. In contrast, the five-hole orifice yielded lower differential pressure and higher-pressure loss compared to the single-hole orifice plate. In case of three-hole orifice plate it performed better than the single-hole orifice with reduced pressure loss and higher differential pressure. It was also found that the power consumed by the pump for pumping was lower for three-hole, four-hole and five-hole orifice plates compared to the single-hole orifice plate. Thus, the three-hole orifice plate performs better than a single-hole orifice plate in terms of higher differential pressure, reduced permanent pressure loss and lower power consumption of the pump.

Keywords: Single-hole and multi-hole orifice plate, differential pressure, permanent pressure loss, pump energy assessment.

1. INTRODUCTION

Orifice plates can be considered ubiquitous devices in fluid flow monitoring and control applications. ISO 5167-1:2003 standard outlines the general installation procedure and the uncertainty linked to flow rate measurement [1] for these restricted devices. Despite being one of the oldest flow measurement instruments, orifice flow meters are still in use today due to their resilience, compact design, reliability, ease of use and maintenance. It is believed that at least 40% of industrial flowmeters in use today are differential pressure based devices, with orifice plates appearing to be the most popular for accurate flow measurement [2].

Many researchers have worked on the development of orifice plates. Sheikh Nasiruddin and S. N. Singh [3] used curved surfaces on both sides of the orifice plate and evaluated its performance using Computational Fluid Dynamics (CFD). The newly designed orifice plate had a better discharge coefficient compared to the reference orifice with a β-value of 0.6 and a radius of curvature of 7.07 mm. It is almost independent of the Reynolds number over the entire range of flow conditions ($10^3 \leq Re \leq 10^6$). R. K. Singh et al. [4] have studied the effect of plate thickness on the Discharge Coefficient (Cd). It was also shown that the orifice plate bevel angle has only a trivial effect on the discharge coefficient for different plate thicknesses. The average discharge coefficient was higher for a 45° bevel angle than for a 30° bevel angle. In an experimental study, Hareth Maher Abd et al. [5] evaluated the flow characteristics of plastic acrylic orifice plate for different beta ratios and Reynolds numbers. It was concluded that the beta ratio has a positive effect on the discharge coefficient for laminar flow, while it has inverse effects on pressure head losses; this, emphasizes the importance of designing the geometric parameters to achieve the desired objective.

Zh. A. Dayev and A. K. Kairakbaev [6] have worked on the positioning of the orifice pressure taps. Based on the geometric flow equations, they have determined the coefficient of contraction and experimentally shown that there is a strong agreement between the coefficient of contraction and the relative diameter of the orifice plate. Thus, it helps in calculating the distances for the pressure taps. T. J. Tharakan and T. A. Rafeeque [7] studied the flow characteristics of 10 sharp-edged orifices with different length-to-diameter ratios in the presence and absence of back pressure. The experiment showed that the radius of the sharp edge of the orifice plates has a significant effect on the discharge coefficient. S. B. M. Beck and J. Mazille [8] developed a new calibration equation for a standard swirl condition introduced before the orifice plate. The results showed that the measurements remain undisturbed regardless of the upstream disturbance.

DOI: 10.2478/msr-2023-0029

Corresponding author: harigurutm07@gmail.com (Hariguru TM)

Perumal Kumar and Michael Wong Ming Bing [9] have created various geometric perforations on a slotted orifice flow meter and compared them with the standard orifice meter. Numerical calculations show that the designed metre is insensitive to the upstream flow profile, with minimal head loss and faster pressure recovery. Studies on the performance of perforated plates, which are often used in pipeline systems to reduce non-uniform flow or to delay the development of cavitation, have also shown that a perforated aperture aids in the precise monitoring of flow rates. Orifice thickness, porosity, hole distribution and upstream disturbance were tested on different topologies. The discharge coefficient of the perforated orifice was 22.5% to 25.6% higher and with less scatter than that of the corresponding conventional orifice [10], [11]. José A. Barros Filho et al. [12] studied the effect of chamfer geometry, which can significantly reduce the pressure drop. The study outlines the creation and testing procedure using CFD to accurately predict the pressure drop across the perforated thin chamfered orifice plates. The validation was done using a collection of plates with different chamfer geometric parameters such as position, angles and sizes. Tianyi Zhao et al. [13] conducted a series of throttle tests and showed how different geometric features change the pressure loss characteristics in a multi-hole orifice plate. Finally, a generalised model for calculating the pressure loss coefficient in a multi-hole orifice plate is presented.

V. K. Singh and T. John Tharakan [14] performed the CFD analysis on a single and multi-hole orifice plate for a range of Reynolds numbrs from 500 to 20000.The experimental results also revealed that the multi-hole orifice flow meter outperformed the single-hole orifice flow meter in terms of higher-pressure recovery and discharge coefficient. In another study [15], [16], the authors analysed the traditional single-hole orifice flowmeters with multi hole orifice plates with the same β-ratios for pneumatic process media. It was demonstrated that certain disadvantages, such as greater pressure drop, delayed pressure recovery and lower discharge coefficient can be mitigated by using a multi-hole orifice plate. However, it was emphasized that further research is needed. Muhammad Asim Mehmood et al. [17] used a commercial computational fluid dynamics code (ANSYS Fluent) to investigate the effects of various geometric parameters on the pressure loss coefficient when using a central composite design, such as the number of holes, the multi-hole diameter ratio and the compactness of the holes. The simulation results show that the pressure loss coefficient is a strong function of the multi-hole diameter. Aneeq Raheem et al. [18] evaluated the performance of single and multi-hole orifice in a 4.5-inch acrylic pipe based on the number of holes, equivalent diameter ratio, compactness ratio, plate thickness ratio and upstream developing length for the Reynolds number range of 24,500 to 55,500. It is shown that the effect is modest for the multi-hole orifice plate. A. Abou El-Azm Aly et al. [19] reported the experimental results by measuring the pressure drop across the fractal-shaped orifices at different pressures. It is shown that the pressure drops across fractal-shaped orifices are smaller than pressure drops across normal circular orifices in the same flow regions. Amra Hasec et al. [20] studied the effect of contamination on the pressure taps to show that when there is contamination, the discharge coefficient is increased, resulting in a negative measurement error regardless of the Reynolds number. The multi-hole orifice metre was shown to be less sensitive to pressure drop fluctuations induced by an increase in the contamination angle compared to single-hole orifice metres.

Most research articles reported are based on CFD simulation and for low Reynolds numbers. In this paper, experimental work was carried out to assess the performance of a multi-hole orifice plate suitable for a three-inch water pipe in terms of differential pressure across the orifice, permanent pressure loss and energy consumption of the VFD pump.

2. METHODOLOGY

A. Design of geometric parameter of the orifice plate

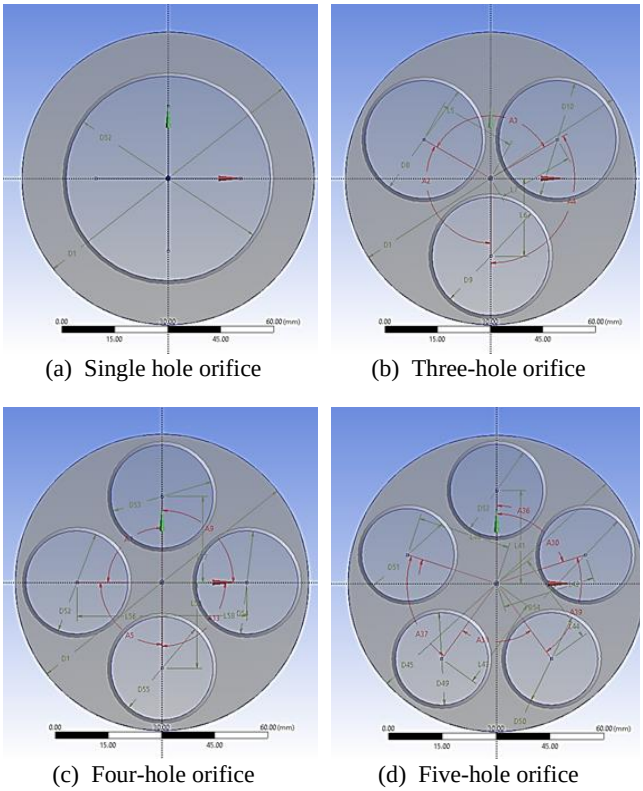

(a) Single hole orifice (b) Three-hole orifice

(c) Four-hole orifice (d) Five-hole orifice

Fig. 1. Orifice geometry.

The single-hole orifice plate is designed to handle a maximum flow rate of 80 m^3/h at a differential pressure of 7500 mm of WC. Fig. 1(a) - Fig. 1(d) shows a single-hole, three-hole, four-hole and five-hole orifice plates. The orifice plates were designed to have the same cross-sectional area (2621.26 mm^2). The thickness of each plate is 3.175 mm [21] and the thickness to diameter ratio [18] (s/d) is 0.05495. The bevel angle is set to 45° with a beta ratio of 0.69771. The diameter of a single-hole orifice plate is 57.77 mm (D52) and the cross-sectional area is 2621.26 mm^2. For a three-hole orifice plate, the diameter is 33.354 mm (D8, D9, D10) and the cross-sectional area of each hole is 873.75 mm^2. The angle between the individual orifice holes (A2, A3, A4) is 120°. For a four-hole orifice, the distance between the centre of the orifice plate and the centre of each orifice hole is

22 mm (L55, L56, L57, L58) and the angle between each orifice plate is 90° (A5, A7, A9, A13). The diameter (D52, D53, D54, D55) of each hole is 28.8 mm and the cross-sectional area of each hole is 655.31 mm^2. For a five-hole orifice plate, the diameter of each hole (D49, D50, D51, D52, D54) is 25.8 mm and the cross-sectional area of each hole is 524.25 mm^2. L40, L41, L42, L43 and L44 indicate the distance between the centre of the orifice plate and the centre of the hole. The angle between each orifice plate is 72° (A30, A36, A37, A38, A39).

B. Computational mesh

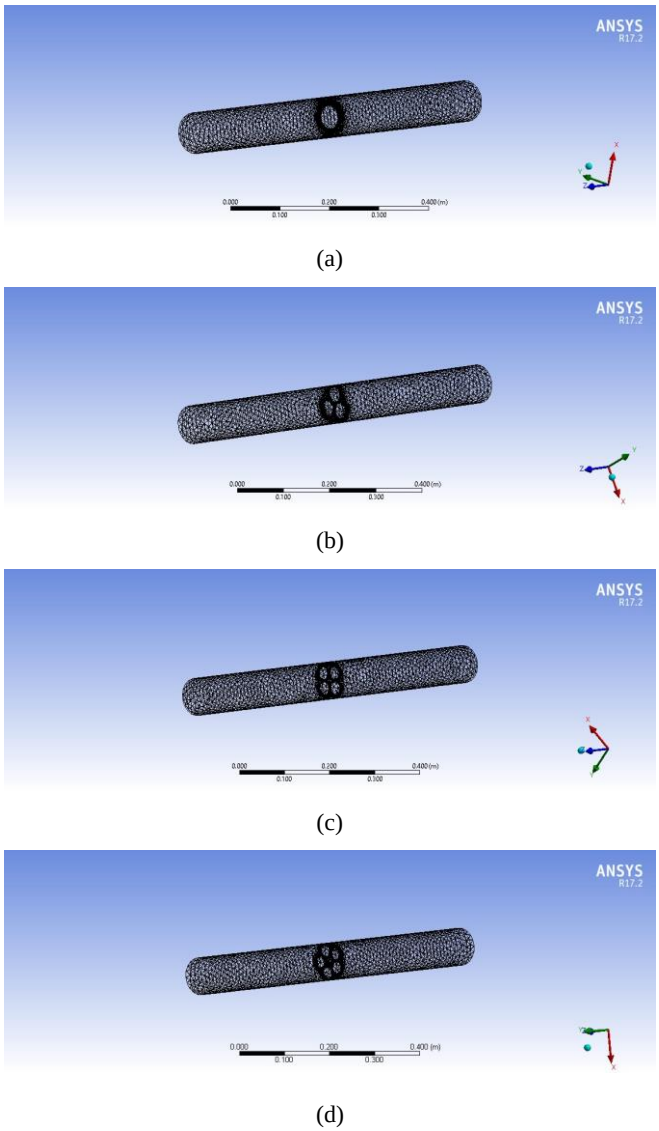

(a) (b) (c) (d)

Fig. 2. Typical grid generated for different Orifice plates (a) Single-, (b) Three-, (c) Four-, (d) Five-hole.

The simulation tool ANSYS Fluent 17.2 [22] is used to simulate the flow through the pipeline for different orifice plates. In Fig. 2, an unstructured tetrahedral mesh was chosen for the entire domain, and its size is defined by the proximity and curvature functions. In the software, the parameters for the pressure-velocity coupling were chosen as follows: Scheme: simple, gradient: least squares cell-based, standard, pressure: second order, momentum: second order upwind, turbulent kinetic energy: first order upwind technique and turbulent dissipation rate: first order upwind. The boundary conditions for the CFD simulations were chosen to make the pipe wall smooth by creating an inflation layer along the walls of the pipeline. The following inlet velocities were set: 1.24 m/s, 1.52 m/s, 1.78 m/s, 2.05 m/s, 2.31 m/s, 2.56 m/s to obtain the following flow rates: 6.1 m^3/h, 7.4 m^3/h, 8.7 m^3/h, 10 m^3/h, 11.3 m^3/h, 12.5 m^3/h. A single model is not sufficient to represent different types of orifice plate arrangements. After some preliminary tests, the final mesh sizes for different orifice plates were obtained as shown in Table 1.

Table 1. Mesh data for the computational domain.

Orifice Type	Number of Nodes	Number of Elements
Single-hole	49740	238816
Three-hole	39534	172169
Four-hole	46021	202333
Five-hole	84002	398859

C. Governing equation for the CFD model

All the governing equations were solved individually and all solutions were considered to be fully converged if each residual was less than 10-4. The turbulent flow through the single-hole and multi-hole orifices is governed by the Reynolds Averaged Navier-Stokes (RANS) equations. A partial differential equation describing the flow of incompressible fluids in fluid mechanics is described below:

Continuity equation

$$\frac{\partial \rho}{\partial t} + \nabla(\rho v_j) = 0 \tag{1}$$

Momentum equation

$$\frac{\partial}{\partial t}(\rho v_j) + \nabla(\rho v_j v_j) = -\nabla p + \nabla \tau \tag{2}$$

In the above equations, p is the Pressure Gradient, v_j is the velocity, τ is the viscous stress tensor, ρ is the density. The fluid pressure in a given geometry is predicted by solving (1) and (2) for a given set of boundary conditions (such as inlets, outlets and walls). These equations have a small number of analytical solutions due to their complexity. Erdal and Anderson [23] discuss the advantages of using the traditional $k-\varepsilon$ turbulence model in numerical predictions for orifice meters. Moreover, Manish et al. [24] and Kumar et al. [9] have successfully used this model for numerical simulation of flows through orifices. Therefore, in this study, the standard $k-\varepsilon$ turbulence model is used for calculations. The following are the governing equations for the standard $k-\varepsilon$ model (3)

$$\frac{\partial(\rho k)}{\partial t} + \frac{\partial(\rho k v_j)}{\partial x_i} = \frac{\partial}{\partial x_j}\left[\left(\mu + \frac{\mu_t}{\sigma_k}\right)\frac{\partial k}{\partial x_j}\right] + G_k - \rho\varepsilon \tag{3}$$

The dissipation rate (ε) of a turbulent model is expressed in (4)

$$\frac{\partial(\rho\varepsilon)}{\partial t}+\frac{\partial(\rho\varepsilon v_j)}{\partial x_i}=\frac{\partial}{\partial x_j}\left[\left(\mu+\frac{\mu_t}{\sigma_\varepsilon}\right)\frac{\partial\varepsilon}{\partial x_j}\right]+C_{1\varepsilon}\frac{\varepsilon}{k}G_k-C_{2\varepsilon}\rho\frac{\varepsilon^2}{k} \quad (4)$$

where

$$G_k=\mu_t S^2-\frac{2}{3}\rho k\Delta v_j-\frac{2}{3}\mu_t(\Delta v_j)^2$$

In this case, G_k represents turbulent kinetic energy as a result of the mean velocity gradient and μ_t represents eddy viscosity

$$\mu_t=\rho C_\mu\frac{\varepsilon^2}{k} \quad (5)$$

The equations also consist of some adjustable constants - σk*, σЄ*, C1Є and C2Є. The values of these constants were obtained by numerous iterations of data fitting for a wide range of turbulent flows. They are as follows: Cμ = 0.09, σk = 1.00, σЄ = 1.30, C1Є = 1.44 and C2Є = 1.92.

3. Experimental setup

The Piping and Instrumentation diagram of the experimental setup is depicted in Fig. 3. The 3-inch stainless steel pipe has a total length of 5.6 metres and consists of a flow straightener, a flanged type orifice plate, a turbine flowmeter and a control valve in series. The differential pressure transmitter connected across the orifice plate has an accuracy of ± 0.05%, a stability of 0.1% and a maximum differential pressure of 10,000 mm of WC. In addition, three pressure transmitters are connected in the setup to measure i) the upstream pressure (P2) at 440 mm upstream of the orifice, ii) the downstream pressure (P4) at 670 mm downstream of the orifice and the orifice taps downstream pressure (P3) calculated from the difference between the pressure across DPT and the pressure point P2.

The turbine flowmeter, which has an accuracy of ±0.15%, is considered to be the true value. The water flow is regulated by a Variable Frequency Drive (VFD) controlled submersible pump, ranging from 51 m^3/h to 24 m^3/h. All field devices were also connected to the Centum VP Yokogawa Distributed Control System (DCS). The experimental setup is shown in Fig. 4.

Fig. 5 shows the DCS graphical view of the measurement setup. The water level in the tank is monitored with an ultrasonic level transmitter (SLT02). Fig. 5 shows the other measurement points, namely the temperature transmitter (3WTT as TT01), the pressure transmitter (3WPT as PT01), the pressure transmitter (1APT as PT02), the differential pressure transmitter (3WDPT as FT01), the pressure transmitter (1WPT as PT04), the turbine flow transmitter (3WTFT as TFT01) and the control valve (3WFCV as FCV01). The orifice flow totalizer (3WDPT totalizer), turbine flow totalizer (3WTFT Totalizer) and differential pressure (3WDPPI as DPT01) across the orifice were also calculated and displayed.

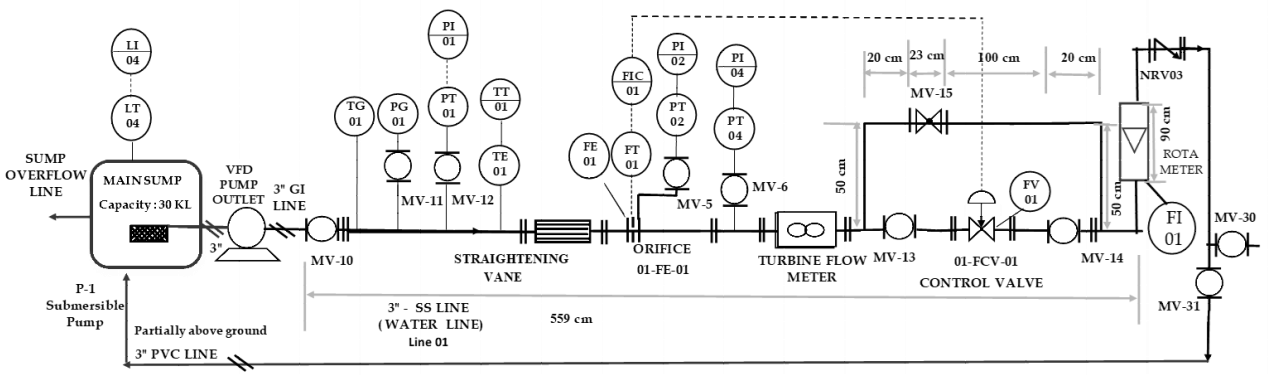

Fig. 3. Piping and Instrumentation diagram of the experimental setup.

Fig. 4. Experimental setup.

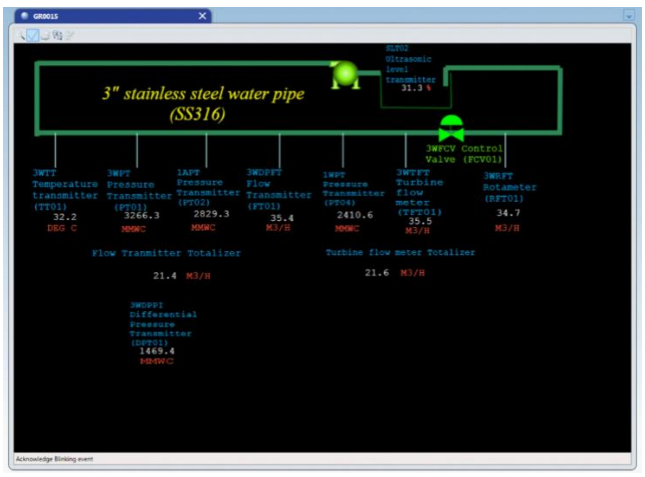

Fig. 5. DCS graphical view.

4. RESULTS AND DISCUSSION

The experiment was carried out for the single-, three-, four- and five-hole orifice plates. The flow rate through the pipe was varied by adjusting the frequency of the VFD from 25 to 50 Hz in steps of 5 Hz. The experimental data flow rate, pressure (P_1, P_2, P_4), differential pressure, turbine flow totalizer, orifice flow totalizer and power consumed by the VFD were recorded for 15 minutes using the DCS and the trend graph is shown in Fig. 6(a) and Fig. 6(b). Table 2 presents the experimental results of the single-, three-, four- and five-hole orifice plate assembly systems.

Fig. 6(a) shows the data acquired from the differential flow transmitter (3WDPT.PV), the turbine flowmeter (3WTFT.PV), the totalized flow across the orifice (3WDPFT.SUM) and the turbine flowmeter (3WTFT.SUM). Fig. 6(b) shows the data obtained from the pressure transmitters P_1, P_2, P_4 and the differential pressure across the orifice plate (3WPT.PV, 1APT.PV, 1WPT.PV, 3WDPPI.PV, respectively).

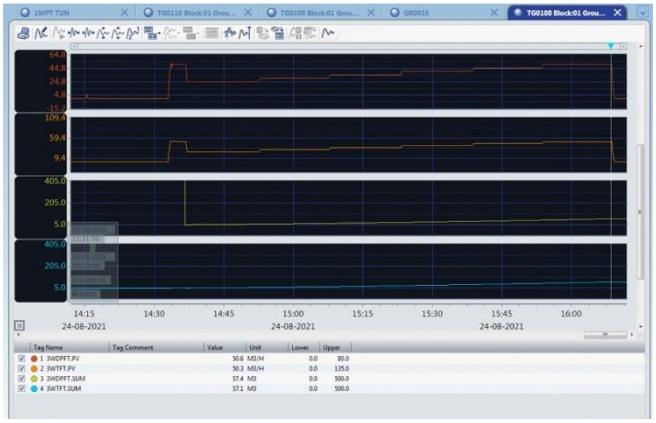

(a)

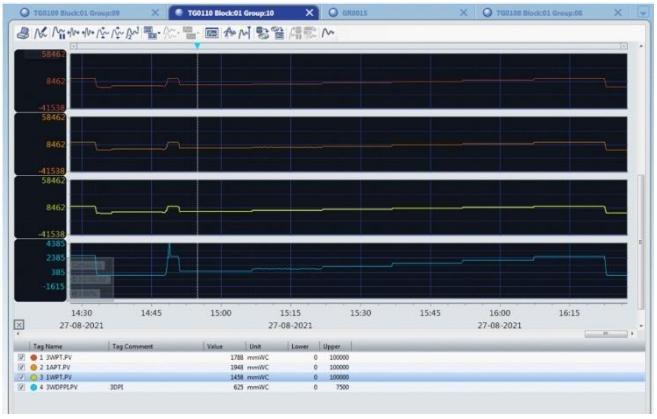

(b)

Fig. 6. (a) and (b), experimental data collected from DCS.

The experimental data obtained may contain some spurious/noisy data that needs to be removed. The box plot [25], as shown in Fig. 7(d), was applied to the entire set of collected data and outliers were removed before calculating the average value. To determine the outlier, the interquartile range was multiplied by 1.5. The calculated value is added with the first and third quartile and all data below or above these calculated values are considered as outliers. The interquartile range is 7 and is multiplied by 1.5 to get 10.5. When added to the first quartile and the third quartile, three data points are found to be out of range and removed as outliers.

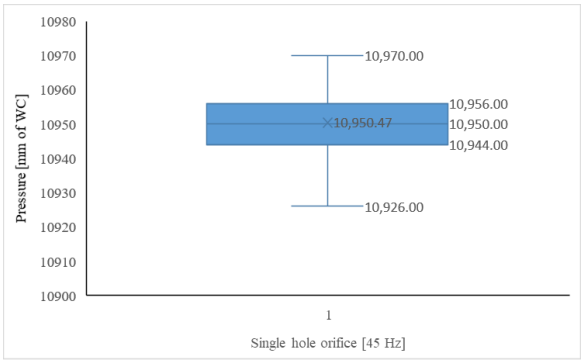

(a)

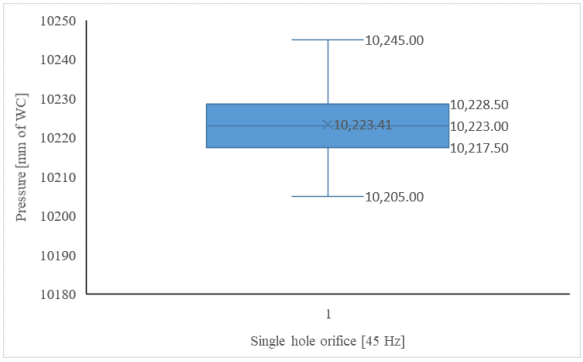

(b)

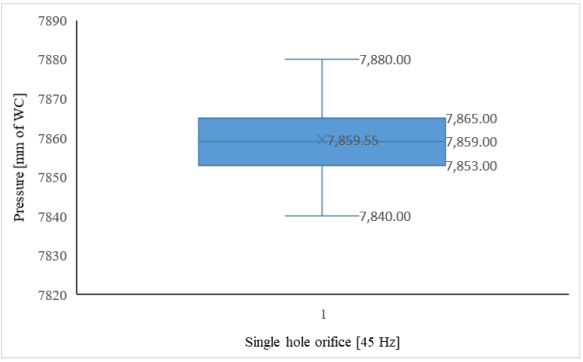

(c)

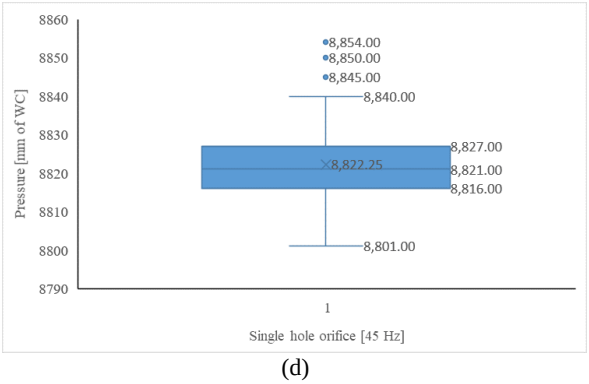

(d)

Fig. 7. Box plot for upstream and downstream pressure (a) P_1, (b) P_2, (c) P_3, (d) P_4.

Table 2 presents the differential pressure measured across the orifice plate when the VFD pump was operated in 5 Hz steps from 25 Hz to 50 Hz. The permanent pressure loss is calculated by subtracting the orifice upstream pressure (P1) from the recovered pressure (P4). Table 2 shows that the totalized flow in both turbines and through the orifice plate is the same. Furthermore, the flow rate through the different sets of orifice plates remained the same for a given operating frequency of the pump.

To calculate the relative difference between a single-hole orifice and multi-hole orifices, the percentage change is determined as

$$\frac{A - B}{\frac{A + B}{2}} \times 100 \quad (6)$$

where

A = Multi-hole orifice

B = Single-hole orifice

Table 2. Experimental results of orifice plate assembly system.

VFD Operating Frequency [Hz]	Totalizer [m^3]		Differential Pressure across the orifice plate [mm of WC]				Permanent pressure loss across the orifice plate [mm of WC]			
	Orifice	Turbine	Single-hole	Three-hole	Four-hole	Five-hole	Single-hole	Three-hole	Four-hole	Five-hole
25	6.1	6.1	685.44	696.38	690.14	672.02	524.39	513.16	539.00	551.98
30	7.4	7.4	1019.48	1036.47	1022.25	999.93	847.20	819.40	877.59	864.93
35	8.7	8.7	1412.40	1435.12	1414.98	1386.93	1221.72	1195.02	1255.19	1243.16
40	10.0	10.0	1861.21	1890.31	1858.57	1824.49	1645.97	1618.51	1665.66	1667.61
45	11.3	11.3	2363.58	2401.99	2364.75	2321.35	2128.99	2103.30	2151.78	2155.98
50	12.5	12.5	2917.16	2970.79	2917.33	2872.66	2652.37	2627.91	2676.61	2691.57

Table 3 shows the percentage change between the single-hole and multi-hole orifice plate in terms of differential pressure across the orifice, permanent pressure loss and power consumption of the VFD pump.

It can be observed that the differential pressure across the three- and four-hole orifice plate is slightly higher compared to the single-hole orifice plate. However, in the case of the five-hole orifice plate, the differential pressure is lower than the single-hole orifice plate. Hence, it demonstrates that the three- and four-hole orifice plates perform better than the single-hole orifice in terms of differential pressure. This is mainly due to the geometric design of the orifice plate. In a three-, four- and five-hole orifice there is a centre obstruction and the holes are on the outer perimeter of the plate. A central circle is drawn to fit within the obstruction region and the diameters of the circles obtained were 7.9532 mm, 16.908 mm and 23.736 mm for three-, four- and five-hole orifice plates, respectively. The number of holes in the orifice plate and the centre obstruction region play a crucial role in the generation of the differential pressure.

The permanent pressure loss across four- and five-hole orifice plates is greater than for the single-hole orifice, but less for the three-hole orifice. Although the three- and four-hole orifice plates had a higher differential pressure than the single-hole orifice plate, the four-hole orifice had a higher permanent pressure loss than the single-hole orifice. Compared to all multi-hole orifice plates, the three-hole orifice plate performed better with a slightly lower pressure loss by 25 mm of WC.

Table 3. Percentage change between the orifice plate assembly system.

Flow rate Q [m^3/min]	Percentage Change of differential Pressure between Single-hole and			Percentage Change of permanent pressure loss between Single-hole and			Percentage Change of power consumption between Single-hole and		
	Three-hole	Four-hole	Five-hole	Three-hole	Four-hole	Five-hole	Three-hole	Four-hole	Five-hole
6.1	2.1647	-2.7478	-5.1264	-1.5834	-0.6833	1.9772	2.7397	-2.6666	0
7.4	3.3361	-3.5239	-2.0711	-1.6527	-0.2713	1.9362	1.7699	0	-1.7391
8.7	2.2095	-2.7025	-1.7396	-1.5957	-0.1825	1.8197	2.3809	3.5928	6.0606
10.0	1.6823	-1.1891	-1.3061	-1.5513	0.1419	1.9925	0.8298	2.5104	-0.8230
11.3	1.2140	-1.0647	-1.2597	-1.6119	-0.0494	1.8028	1.8237	1.2121	-3.5503
12.5	0.9264	-0.9097	-1.4670	-1.8216	-0.0058	1.5371	4.8565	1.7391	2.1786

The power consumed by the VFD-operated pump under different flow conditions and with different sets of orifice plates was also investigated. Table 4 and Fig. 8 show the power consumed by the pump over 15 minutes and it can be seen that using a multi-hole orifice consumes less power than using a single-hole orifice. When the total power consumption of the different multi-hole orifices was compared, the three-hole orifice consumed less power. Compared to a single-hole orifice, the power consumed by a three-hole orifice is lower, ranging from 1 to 10 kWh depending on the flow conditions.

Table 4. Power consumption by VFD pump.

VFD Operating Frequency [Hz]	Power consumed by VFD pump (KW)			
	Single-hole orifice	Three-hole orifice	Four-hole orifice	Five-hole orifice
25	35.52	34.56	36.48	35.52
30	54.72	53.76	54.72	55.68
-35	81.60	79.68	78.72	76.80
40	116.16	115.20	113.28	117.12
45	159.36	156.48	157.44	165.12
50	222.72	212.16	218.88	217.92

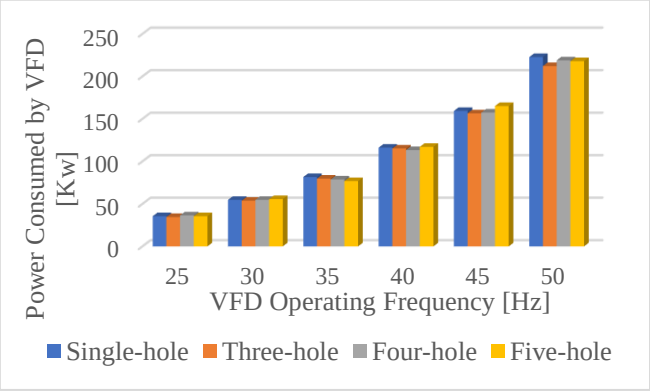

Fig. 8. Power consumption by VFD pump.

The pressure distribution across the pipeline for the different sets of orifice plates is shown in Fig. 9. It can be observed that the upstream pressure variation depends on the type of orifice plate. For a single-hole orifice, the maximum pressure is observed at the circumference of the pipe, for a three-hole orifice it is on top of the pipe, for a four-hole orifice at the centre of the plate and for a five-hole orifice at the circumference of the plate and at the centre of the plate. Similarly, in the case of downstream pressure, higher pressure is observed for the single-hole orifice plate compared to the multi-hole orifice plate (-2.3e+3 Pa for the single-hole, -3.8e+3 Pa for the three-hole, -4.4e+3 Pa for the four-hole, and -5.0e+3 Pa for the five-hole orifice).

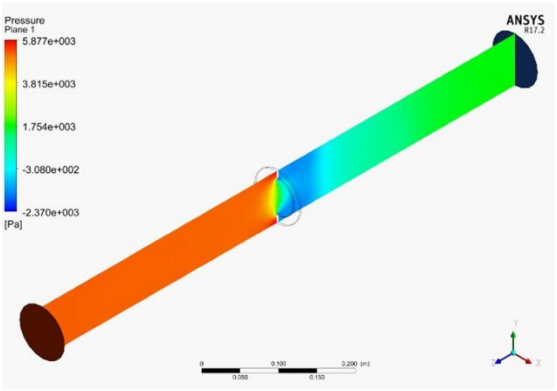

(a)

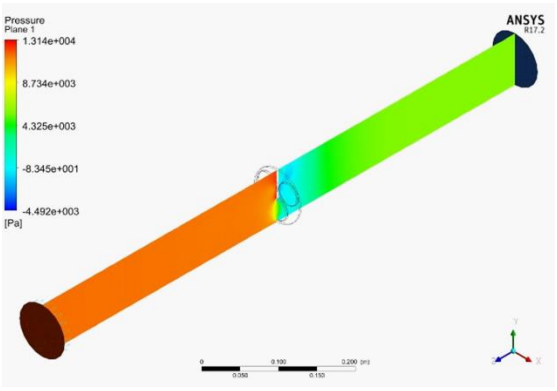

(b)

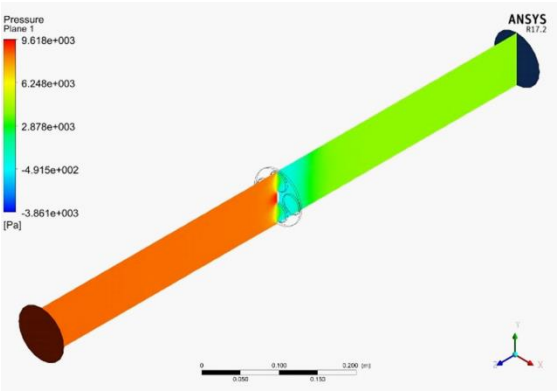

(c)

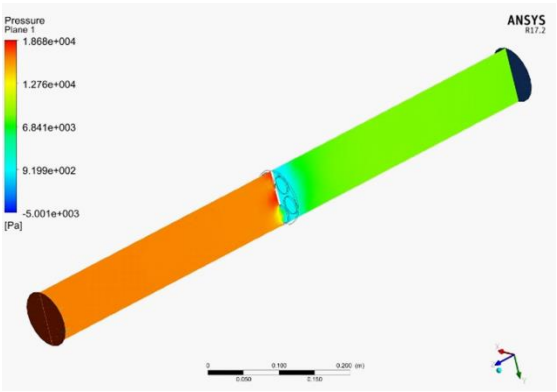

(d)

Fig. 9. Pressure distribution across a different set of orifice plates (a) Single-, (b) Three-,(c) Four- and (d) Five-hole.

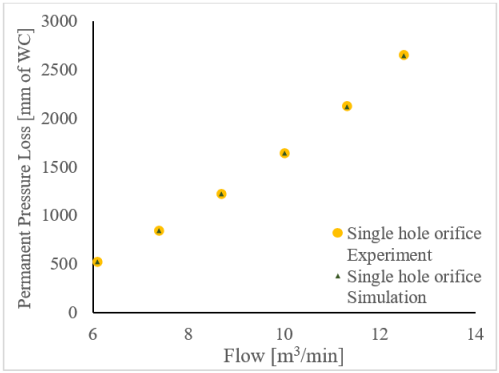

(a)

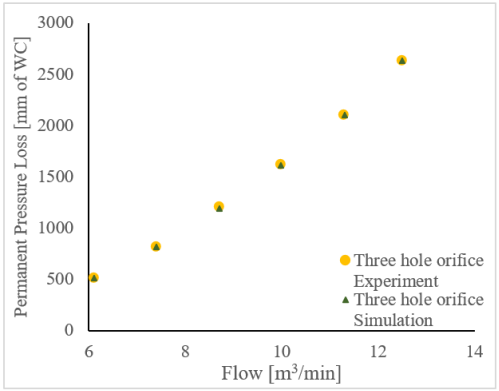

(b)

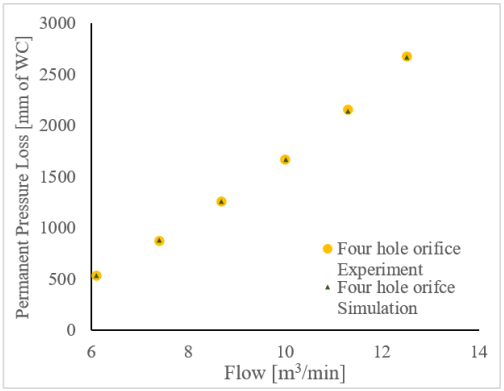

(c)

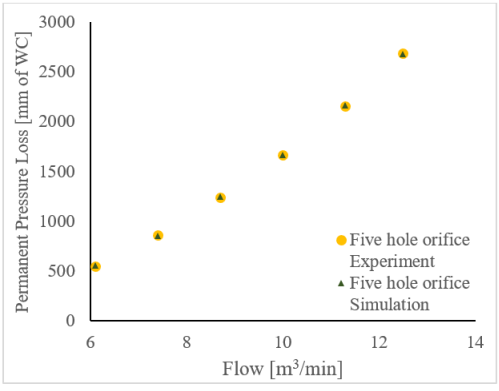

(d)

Fig. 10. Comparison of permanent pressure loss between simulation and experiment setup (a) Single-, (b) Three-, (c) Four-, (d) Five-hole.

Table 5 shows the permanent pressure loss based on the simulation of the single-, three-, four- and five-hole orifice plates. It can be seen that the permanent pressure loss across the three-hole orifice plate is less than across the single-hole and the other multi-hole orifice plates. Fig. 10 shows the comparison of the experimental and simulation results of the permanent pressure loss for different orifice plates. To determine the deviation between the experimental and simulation results, the percentage change in permanent pressure loss is calculated using (7).

$$\frac{A - B}{A} \times 100 \tag{7}$$

where

A = Experimental value

B = Simulation value

The mean absolute deviations between the experimental and the simulation flow rates for the single-, three-, four- and five-hole orifice plates are 0.306593, 0.317886, 0.599315 and 0.503381, respectively. It can be seen that the simulated permanent pressure losses are slightly lower than the experimental data, as the model was derived for the single-hole orifice plate. However, an ideal model derived for each orifice plate individually gave an identical result to the experimental results.

Table 5. Permanent pressure loss based on simulation.

Flow Rate [m³/min]	Permanent Pressure Loss (mm of WC)			
	Single-hole	Three-hole	Four-hole	Five-hole
6.1	523.82	509.85	531.88	555.94
7.4	853.70	821.38	885.62	858.29
8.7	1227.12	1193.78	1262.61	1252.61
10.0	1646.12	1609.11	1665.09	1667.13
11.3	2127.12	2104.28	2142.01	2165.26
12.5	2648.30	2633.82	2667.27	2683.07

The value of the discharge coefficient can vary depending on the Reynolds number and the pipe diameter [18]. The discharge coefficient is important in the piping system design because it affects the accuracy of flow rate measurements as well as the overall performance of the system.

Table 6 and Fig. 11 show the Reynolds number and the discharge coefficient at different operating conditions. From Table 6 it can be seen that the discharge coefficient for a three-hole orifice is practically constant over the entire operating range compared to other types of orifice plates. The Reynolds number is also lower for three- and four-hole orifice plates than for single-hole orifice and five-hole orifice plates.

Table 6. Calculated Discharge coefficient and Reynolds number for different orifice plates.

Flow [Q]	Single-hole orifice plate		Three-hole orifice plate		Four-hole orifice plate		Five-hole orifice plate	
	Discharge Coefficient [C_d]	Reynolds no [Re]	Discharge Coefficient [C_d]	Reynolds no [Re]	Discharge Coefficient [C_d]	Reynolds no [Re]	Discharge Coefficient [C_d]	Reynolds no [Re]
6.1	0.6087	129060.37	0.6033	128929.42	0.6068	129093.57	0.6144	128976.32
7.4	0.6084	157303.36	0.6026	157093.16	0.6070	157169.37	0.6137	157151.78
8.7	0.6080	185051.70	0.6030	184975.49	0.6072	184957.90	0.6129	184834.79
10.0	0.6079	212366.16	0.6028	212230.53	0.6074	212048.79	0.6131	212054.65
11.3	0.6078	239307.96	0.6028	239239.35	0.6072	239127.96	0.6128	239104.51
12.5	0.6075	265696.52	0.6028	266078.14	0.6073	265626.73	0.6130	266048.83

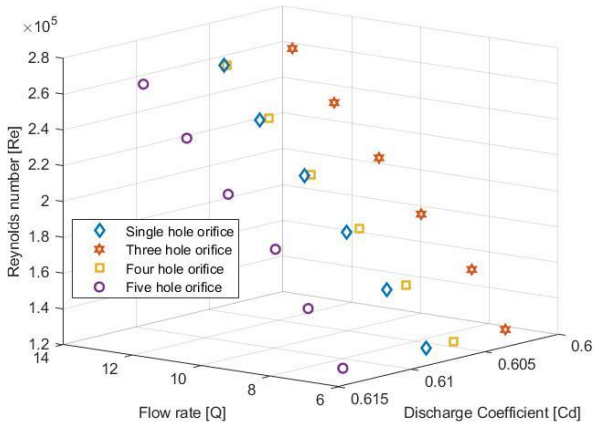

Fig. 11. The relationship between discharge coefficient, Reynolds number, and flow rate for various orifice plates.

5. Conclusion

The performance of the single-hole and multi-hole orifice plates in terms of differential pressure across the orifice plate and permanent pressure loss is evaluated using ANSYS software. The differential pressure and permanent pressure loss across the orifice plate were recorded in real-time setup with an orifice plate having a beta ratio of 0.69771. The simulation results agree with the experimental results in terms of differential pressure and are slightly lower in terms of permanent pressure loss as the model was derived for the single-hole orifice plate. However, a separate model for each orifice plate results in a perfect match between the simulation and the experimental result.

In the experimental setup the flow rate is controlled by a variable frequency drive pump, varied from 24 m^3/h to 51 m^3/h. The measurement was taken for 15 minutes to obtain a steady state reading, and all outliers were removed. The flow rate, differential pressure across the orifice plate, permanent pressure loss and pump power consumption were measured in the DCS. The results show that the four-hole orifice plate produced a larger differential pressure and a higher-pressure loss, and the five-hole orifice produced a lower differential pressure and a higher-pressure loss than the single-hole orifice plate. However, the three-hole orifice plates outperformed the single-hole orifice plates in terms of lower pressure loss and higher differential pressure. The power consumption of the pump is lower when a multi-hole orifice plate is connected in the line then when a single-hole orifice plate is connected. In addition, the discharge coefficient of a three-hole orifice is almost constant over the entire operating range compared to other types of orifice plates. As a result, three-hole orifice plates outperform single-hole orifice plates in terms of slightly higher differential pressure (1.92216 ± 0.859206), lower permanent pressure loss (-1.6361 ± 0.096821) and lower power consumption (2.40008 ± 1.367101).

References

[1] ISO. (2003). *Measurement of fluid flow by means of pressure differential devices inserted in circular cross-section conduits running full — Part 1: General principles and requirements*. ISO 5167-1:2003. https://www.iso.org/standard/28064.html

[2] Reader-Harris, M. (2015). *Orifice Plates and Venturi Tubes*. Springer, ISBN 978-3319168791.

[3] Nasiruddin, S., Singh, S. N. (2021). Performance evaluation of an innovative design modification of an orifice meter. *Flow Measurement and Instrumentation*, 80, 101944. https://doi.org/10.1016/j.flowmeasinst.2021.101944

[4] Singh, R. K., Singh, S. N., Seshadri, V. (2010). Performance evaluation of orifice plate assemblies under non-standard conditions using CFD. *Indian Journal of Engineering & Materials Sciences*, 17, 397-406.

[5] Abd, H. M., Alomar, O. R., Mohamed, I. A. (2019). Effects of varying orifice diameter and Reynolds number on discharge coefficient and wall pressure. *Flow Measurement and Instrumentation*, 65, 219-226. https://doi.org/10.1016/j.flowmeasinst.2019.01.004

[6] Dayev, Z. A., Kairakbaev, A. K. (2019). Modeling of coefficient of contraction of differential pressure flowmeters. *Flow Measurement and Instrumentation*, 66, 128-131. https://doi.org/10.1016/j.flowmeasinst.2019.02.009

[7] Tharakan, T. J., Rafeeque, T. A. (2016). The role of backpressure on discharge coefficient of sharp edged injection orifices. *Aerospace Science and Technology*, 49, 269-275. https://doi.org/10.1016/j.ast.2015.12.014

[8] Beck, S. B. M., Mazille, J. (2002). A study of a pressure differential flow meter that is insensitive to inlet conditions. *Flow Measurement and Instrumentation*, 12 (5-6), 379-384. https://doi.org/10.1016/S0955-5986(01)00034-6

[9] Kumar, P., Ming Bing, M. W. (2011). A CFD study of low pressure wet gas metering using slotted orifice meters. *Flow Measurement and Instrumentation*, 22 (1), 33-42. https://doi.org/10.1016/j.flowmeasinst.2010.12.002

[10] Huang, S., Ma, T., Wang, D., Lin, Z. (2013). Study on discharge coefficient of perforated orifices as a new kind of flowmeter. *Experimental Thermal and Fluid Science*, 46, 74-83. https://doi.org/10.1016/j.expthermflusci.2012.11.022

[11] Malavasi, S., Messa, G., Fratino, U., Pagano, A. (2012). On the pressure losses through perforated plates. *Flow Measurement and Instrumentation*, 28, 57-66. https://doi.org/10.1016/j.flowmeasinst.2012.07.006

[12] Barros Filho, J. A., Santos, A. A. C., Navarro, M. A., Jordão, E. (2015). Effect of chamfer geometry on the pressure drop of perforated plates with thin orifices. *Nuclear Engineering and Design*, 284, 74-79. https://doi.org/10.1016/j.nucengdes.2014.12.009

[13] Zhao, T., Zhang, J., Ma, L. (2011). A general structural design methodology for multi-hole orifices and its experimental application. *Journal of Mechanical Science and Technology*, 25, 2237-2246. https://doi.org/10.1007/s12206-011-0706-3

[14] Singh, V. K., Tharakan, T. J. (2015). Numerical simulations for multi-hole orifice flow meter. *Flow Measurement and Instrumentation*, 45, 375-383. https://doi.org/10.1016/j.flowmeasinst.2015.08.004

[15] Đurđević, M., Bukurov, M., Tašin, S., Bikić, S. (2019). Experimental research of single-hole and multi-hole orifice gas flow meters. *Flow Measurement and Instrumentation*, 70, 101650. https://doi.org/10.1016/j.flowmeasinst.2019.101650

[16] Đurđević, M., Bukurov, M., Tašin, S., Bikić, S. (2020). Numerical study of single-hole and multi-holes orifice flow parameters. *Journal of Applied Fluid Mechanics*, 14, 215-226. https://doi.org/10.47176/jafm.14.01.31472

[17] Mehmood, M. A., Ibrahim, M. A., Ullah A., Inayat, M. H. (2019). CFD study of pressure loss characteristics of multi-holed orifice plates using central composite design. *Flow Measurement and Instrumentation*, 70, 101654. https://doi.org/10.1016/j.flowmeasinst.2019.101654

[18] Raheem, A., Siddiqi, A. S. B., Ibrahim, A., Ullah, A., Inayat, M. H. (2021). Evaluation of multi-holed orifice flowmeters under developing flow conditions – An experimental study. *Flow Measurement and Instrumentation*, 79, 101894. https://doi.org/10.1016/j.flowmeasinst.2021.101894

[19] El-Azm Aly, A. A., Chong, A., Nicolleau, F., Beck, S. (2010). Experimental study of the pressure drop after fractal-shaped orifices in turbulent pipe flows. *Experimental Thermal and Fluid Science*, 34 (1), 104-111. https://doi.org/10.1016/j.expthermflusci.2009.09.008

[20] Hasečic, A., Imamovic, J., Bikic, S., Dzaferovic, E. (2021). Investigation of the contamination influence on the parameters of gas flow through multihole orifice flowmeter. *IEEE Transactions on Instrumentation and Measurement*, 70, 7501808. https://doi.org/10.1109/TIM.2021.3063198

[21] Zedan, M. F., Teyssandier, R. G. (1990). Effect of errors in pressure tap locations on the discharge coefficient of a flange tapped orifice plate. *Flow Measurement and Instrumentation*, 1 (3), 141-148. https://doi.org/10.1016/0955-5986(90)90003-P

[22] ANSYS Inc. (2013). *ANSYS FLUENT Theory Guide*, 724.

[23] Erdal, A., Andersson, H. I. (1997). Numerical aspects of flow computation through orifices. *Flow Measurement and Instrumentation*, 8 (1), 27-37. https://doi.org/10.1016/S0955-5986(97)00017-4

[24] Shah, M. S., Joshi, J. B., Kalsi, A. S., Prasad, C. S. R., Shukla, D. S. (2012). Analysis of flow through an orifice meter: CFD simulation. *Chemical Engineering Science*, 71, 300-309. https://doi.org/10.1016/j.ces.2011.11.022

[25] Hubert, M., Vandervieren, E. (2008). An adjusted boxplot for skewed distributions. *Computational Statistics & Data Analysis*, 52 (12), 5186-5201. https://doi.org/10.1016/j.csda.2007.11.008

Received April 14, 2023
Accepted September 25, 2023